# A tale of three taxes: photo-gyro-gravitactic bioconvection

C. R. Williams and M. A. Bees
Department of Mathematics, University of Glasgow, Glasgow G12 8QW, UK
Submitted 13 August 2010

## SUMMARY

**The term bioconvection encapsulates the intricate patterns in concentration, due to hydrodynamic instabilities, that may arise in suspensions of non-neutrally buoyant, biased swimming microorganisms. The directional bias may be due to light (phototaxis), gravity (gravitaxis), a combination of viscous and gravitational torques (gyrotaxis), or other taxes. The aim of this study is to quantify experimentally the wavelength of the initial pattern to form from an initially well-mixed suspension of unicellular, swimming green algae as a function of concentration and illumination. As this is the first such study, it is necessary to develop a robust and meticulous methodology to achieve this end. The phototactic, gyrotactic and gravitactic alga *Chlamydomonas augustae* is employed, with various red or white light intensities from above or below, as the three not altogether separable taxes are probed. Whilst bioconvection was found to be unresponsive to changes in red light, intriguing trends were found for pattern wavelength as a function of white light intensity, depending critically on the orientation of the illumination. These trends are explored to help unravel the mechanisms. Furthermore, comparisons are made with theoretical predictions of initial wavelengths from a recent model of photo-gyrotaxis, encouragingly revealing good qualitative agreement.**

**Keywords**: bioconvection, swimming, microorganism, phototaxis, gyrotaxis

## INTRODUCTION

The term ‘bioconvection’ was coined by Platt to describe self-sustained pattern formation in shallow suspensions of motile microorganisms that are denser than the fluid in which they swim (Platt, 1961). However, bioconvection is one of the earliest observations of collective behaviours of microorganisms (Wagner, 1911). The mechanisms do not necessarily involve communication between the cells. Rather,

external influences, such as light and gravity, and self-induced fluid flow bias the cells' swimming directions. Many microorganism species, such as those belonging to the genus *Chlamydomonas*, are bottom heavy, leading cells to swim upwards on average (gravitaxis); cells tend to accumulate at the upper boundary. If the cells are denser than the surrounding fluid, a horizontal layer with a higher density than the fluid below results. This can lead to Rayleigh-Taylor instabilities, which drive large-scale fluid motion and lead to intricate spatial patterns. Additionally, viscous torques are exerted on each cell by the fluid motion and the combination of these torques together with those due to gravity is termed gyrotaxis (Kessler, 1984). Gyrotaxis causes cells to swim towards regions of locally downwelling and away from upwelling fluid (Kessler, 1985a,b). This is a second mechanism that can lead to instabilities, even in the absence of an upper boundary, since cells swim towards any regions of locally downwelling fluid and their added mass amplifies the downwelling, creating long vertical plumes (Fig. 1a). Both instabilities lead to large scale pattern formation and in shallow suspensions, when viewed from above with bright-field illumination, cells form complex patterns with dark regions indicating high cell concentrations (Fig. 1b).

Many genera of microorganism (e.g. *Chlamydomonas, Dunaliella* and *Euglena*; Nultsch *et al*. 1971) also swim towards weak light (positive phototaxis) and away from strong light (negative phototaxis). This suggests an optimal, or critical, light intensity exists between these two regimes. Self-shading within a population can occur, where cells closer to the light source absorb and scatter the light: the location of the critical light intensity is determined by the distribution of individuals within the fluid layer. In theory, if the light intensity at an upper source is greater than the critical light intensity then cells near the source will swim downwards, while those further away are shaded by cells above and so swim upwards, resulting in a concentrated, dense sublayer of cells. Only the region below the sublayer is gravitationally unstable. A Rayleigh-Taylor instability caused by the density difference between the cells and the fluid can occur (Vincent and Hill, 1996). Penetrative bioconvection can result, where flows from the unstable region penetrate into the stable region and result in motions that occupy the whole fluid layer, analogous to penetrative thermal convection (Veronis, 1963).

The importance of phototrophic algae for biofuel production should not be overlooked. For economic viability of biofuels from algae one should look to reduce the energy input into such systems. Photo-gyrotactic behaviour may help to self-concentrate the cells, direct cells away from vertical boundaries (avoiding surface biofouling), provide greater light penetration into deep suspensions, and mix nutrients and promote gas exchange (potentially replacing or enhancing turbulent stirring in algal biofuel systems). The light location might also be adjusted to block bioconvection.

Various models for gravitactic, gyrotactic or phototactic bioconvection have been proposed. Childress and colleagues presented a continuum model for a finite depth suspension of upswimming cells (Childress *et al*., 1975). The suspension was assumed to be sufficiently dilute so that cell-to-cell interactions could be neglected. Non-Newtonian stresses, such as those associated with swimming strokes, were not considered. The model consisted of the Navier-Stokes equations for the incompressible fluid flow with an additional term for the negatively buoyant cells; and a cell conservation equation, accounting for advection of the cells by the flow, simple up-swimming and isotropic diffusion. Using linear stability analysis, the dominant initial pattern wavelength was predicted to be limited by the size of the container (zero critical wavenumber). However, the discovery of gyrotaxis demonstrated the incompleteness of this description and injected new energy into theoretical investigations, with subsequent models explicitly including gyrotaxis (with gravitaxis implicit). The first models calculated cell swimming direction deterministically and used constant isotropic diffusion (Hill *et al.*, 1989). Later, a refined continuum model was developed (Pedley and Kessler, 1990), with a stochastic gyrotactic description from which the flow-dependent mean cell swimming direction and diffusion tensor could be derived. This model was analysed for a layer of finite depth (Bees and Hill, 1998): finite initial pattern wavelengths were predicted for sufficient gyrotaxis. In the first model of phototactic only cells (Vincent and Hill, 1996), cells simply swam upwards or downwards dependent on the local light intensity (see Ghorai and Hill, 2005). Finally, three models have been constructed that include phototaxis, gravitaxis and gyrotaxis in a continuum description of bioconvection (Williams and Bees, 2010; in the spirit of Pedley and Kessler, 1990).

These represent the first rational models of photo-gyrotaxis and mark a substantial development in the theory of bioconvection under illumination.

There has not been a substantial amount of quantitative experimental work to accompany the theoretical developments; early studies and observations were qualitative in nature (Wager, 1911; Kessler, 1984, 1985b, 1986). More recently, controlled experiments quantified the initial and final wavelengths of patterns as a function of cell concentration and depth in a shallow suspension of *C. augustae* (Bees and Hill, 1997; no phototaxis, as effectively in the dark). The initial wavelengths could be compared with model predictions (Bees and Hill, 1998). Finally, Czirók and colleagues investigated bioconvection in suspensions of aerotactic bacteria (Czirók *et al*., 2000). Combined phototaxis and gravitaxis has been probed in tracking experiments (Kessler et al. 1992) with either weak or strong horizontal irradiance, with the conclusion that "any complete discussion of phototaxis in a microorganism that is also gravitactic must take both responses into account."

The aim of this investigation is to analyse experimentally the effects of light intensity and concentration on the initial wavelength of the pattern in a repeatable and precise manner. This is the very first quantitative study on the effect of light on bioconvection patterns. The initial instability that forms before any higher order, non-linear effects occur is of particular interest as this can be compared directly with theoretical predictions (Williams and Bees, 2010) on photo-gyrotactic bioconvection. The methodology has been developed from the literature (Bees and Hill, 1998; Czirók *et al*., 2000), with some key modifications and extensions. In particular, a novel, automated method of mixing was designed in an attempt to decrease the effects of variable mixing that occur between experiments. Furthermore, this is the first study of its kind systematically to repeat experimental runs, using the same cells, in order to provide a solid statistical basis for the results and mechanistic descriptions. Additionally, each experiment was repeated using different cells to assess whether the trend was repeatable. Fourier analysis is used to extract the dominant initial pattern wavelength as a function of concentration and light intensity, with red and white illumination from above and below. This study concludes with a thorough discussion of the mechanisms responsible for the trends that are observed, and a comparison with theoretical predictions, where, encouragingly, good agreement is found.

## MATERIALS AND METHODS

### Culture, depth and concentration

The experiments were performed with the motile green alga *Chlamydomonas augustae*, strain CCAP 11/51B (previously *C. nivalis* in the literature) suspended in Bold's Basal Medium (BBM). Cultures were stored in 500 mL conical flasks, sealed with cotton wool and covered in tin foil to avoid contamination. Illumination was from above using bright white florescent strip lights (16:8 hours light:dark cycle; intensity of 1900 lux just above the cultures). Cultures were sub-cultured every 4 weeks and used in experiments after 2-4 weeks. The cells can be concentrated by placing sterile absorbent cotton wool in the neck of the flask; cells swim upwards through the cotton wool and accumulate at the top in the dark. After 2 days, a pipette was used to extract a known volume of concentrated culture, which was placed it in a Petri dish of diameter 5.2 cm. To avoid adhesion to the Petri dish, new dishes were washed with distilled water and then culture, followed by concentrated suspension and left for 24 hours. The depth in the centre of the dish was measured using a microscope focus, calibrated with glass slides measured with a micrometer. Concentration was measured using the mean of five colorimeter measurements (WPA CO7500 colorimeter, 590 nm; BBM reference; calibrated via a haemocytometer, using Beer's law to find a linear relationship between absorbance and concentration; non-linearity for high concentrations was avoided by dilution).

### Mixing and lighting

For quantitative studies of bioconvection patterns, a uniform distribution of cells is required in the Petri dish at the start of the experiment, to standardize initial conditions. In previous studies, cultures were mixed by hand (Czirók *et al*., 2000), which allowed patterns to vary between experiments (Fig. 8, Bees and Hill, 1997) due to the inherent ability of the cells to self-concentrate in a range of flows. Here, an automated mixing method was designed and implemented to standardize mixing "to an acceptable degree" between experimental runs. A vortex mixer (Jencons PLS VX100) was used with a flat head attachment to support the culture in the Petri dish positioned on a light box (for light from below) or on a counterbalanced board (for light from above) on top of the mixer. The vortex mixer was set to a slow 200 r.p.m., creating a swirling, sloshing motion in the culture that appeared to mix the

suspension. Mixing was deemed acceptable if the pattern appeared to form uniformly, the pattern appeared after the effects of mixing had subsided and did not obviously follow streamlines. Investigation showed that an initial thorough mixing followed by a rest period and then a further brief mixing satisfied these requirements. The mixing motion varied a little with the position of the illumination. Parameters for each experiment are summarized in Table 1, where consecutive pairs of (mixing, waiting) times are indicated.

Lighting consisted of either a red or cold white uniform diffuse LED array (Advanced Illumination, UK; no significant heating; for spectra, see Williams 2009). All other lights were extinguished. The PC-controlled illumination intensity was stated in lux on the surface of the light box, calibrated with a light meter. For light from below, the culture dish was fixed within a large Petri dish on the light box, for stability, with a lid to reduce contamination and limit evaporation. This in turn was attached to the vortex mixer, with a tripod-mounted camera overhead. For illumination from above, a board was employed with a Petri dish-sized hole at one end: the culture dish was inserted in the hole with the light strapped to the top; the board was attached to the mixer, and counterbalanced, with the inverted camera below.

## Varying concentration in the suspension

Depth and illumination were kept constant for experiments that involved varying concentration. Eight experimental runs were performed with the maximum concentration, $C_{max}$. A controlled dilution was obtained by replacing 2 mL of culture in the Petri dish with 2 mL of BBM (equilibrated temperature), without repositioning the culture. The culture was thoroughly mixed and left on the light box to re-adjust for 10 minutes before performing another eight experimental runs. This procedure was repeated, with 2 mL replaced each time, until pattern formation was significantly attenuated: typically, 5 dilutions were required.

## Image capture and analysis

For each experimental run (mixing plus image capture), thirty images were captured (Camtek low-light-sensitive BW CCD) at intervals of 2 s. For each set of parameter values, $n$ represents the number of experiments (separated by 30 s) performed with the

same cells. Light intensity $I$ was initially set at 645 lux (10 % of maximum) and was increased in increments of 15% of the maximum.

Fourier analysis was employed to extract the dominant wavelength in each of the recorded images (for details and references see Bees and Hill, 1997; Czirók *et al*., 2000). In brief, using software written on the graphics package IDL (RSI), the first image was subtracted from the stack of images to extract unwanted information (the walls of the dish, imperfections, and uneven lighting); a Hahn windowing function was used to eliminate the effects of the sharp edges of the image before Fast-Fourier Transforming (FFT). The FFT takes a real, two-dimensional image array and returns a complex array of the same size containing amplitude and phase information, from which a discrete Fourier spectrum, $G(k)$, for wavenumber $k$ can be computed, yielding the dominant wavenumber. Two functions have been proposed to fit the spectrum (using least-squares): an unnormalized double Gaussian distribution (Bees and Hill, 1997); and a function with power-law decay for both small and large wavenumbers (Czirók *et al*., 2000) of the form

$$\ln[G(k)] = \alpha\left|\ln(k) - \ln(k_d)\right| - \beta\ln(k) + c, \qquad \textbf{(Eqn. 1)}$$

where $k_d$ is the dominant wavenumber (the peak of the fit), and $\alpha$, $\beta$ and $c$ are fitting parameters ($\alpha$ and $\beta$ are exponents for small and large wavenumbers). This is equivalent to separating logarithms and writing

$$G(k) \approx k^{-\alpha-\beta} \text{ when } k < k_d, \text{ and } G(k) \approx k^{\alpha-\beta} \text{ when } k > k_d.$$

For the images herein, the double logarithmic function better fitted the data than the double Gaussian and thus was used throughout (sum modulus and Kolmorgorov-Smirnov statistics were smaller; Williams, 2009). An example of the fitting is shown in Fig. 5. Very occasionally, when poor fitting statistics were obtained, the first most unstable wavenumber was estimated directly from the spectrum (very few cases). Wavenumber can be converted to wavelength $\lambda = W_I / k_d$, where $W_I$ is the image width in cm. The initial dominant wavenumber and wavelength are denoted $k_0$ and $\lambda_0$, respectively, and were identified as such if the associated Fourier spectrum density was sufficiently greater than the noise and grew with time. Finally, the data easily satisfies the Nyquist criterion of at least 2 pixels per oscillation.

## Statistical Analysis

Linear regression analyses were performed (Sigma Plot 8.0) on all data points from each experimental run (not just the mean wavelength). Correlation coefficients were found and T-tests performed to analyse the probability of incorrectly concluding the existence of an association between the dependent and independent variables. Unpaired T-tests were also used, to establish if differences in mean wavelength for different parameters were significant.

# RESULTS

To facilitate easy discussion of the experimental results in the next section we shall employ the experimental naming convention in Table 1.

| **Experiment** | **Light type** | **Light orientation** | **$(m_i,t_i)$ pairs (seconds)** |
|---|---|---|---|
| RA | Red | Above | (4,10),(2,10) |
| CA | White | Above | (5,2),(3,4),(2,10)* |
| CB | White | Below | (2,10),(1,12) |
| $LA_{(1,2,3)}$ | White | Above | (5,2),(3,4),(2,12) |
| $LB_{(1,2,3)}$ | White | Below | (3,10),(1,12) |

Table 1 Summary of the experimental mixing protocol. Labels A and B indicate light from above and below, respectively. R indicates red light, and C and L indicate concentration and white light intensity experiments, respectively. The last column is a sequence of pairs of (mixing, waiting) times: either $(m_1,t_1),(m_2,t_2)$ or $(m_1,t_1),(m_2,t_2),(m_3,t_3)$ in cases where more mixing was required. The star indicates that the final waiting time was flexible, to avoid missing initial pattern formation.

## Exploring the effects of concentration on initial pattern wavelength

Fig. 4 shows two examples of the evolution of bioconvection patterns with illumination from above at 645 lux, for different concentrations. There is a clear difference in the patterns formed: for the higher concentration the pattern has an earlier onset and a smaller wavelength compared to the lower concentration.

Results for the effect of concentration on initial pattern wavelength are shown in Fig. 2, where the data points are the mean of 8 separate measurements of the same cells and the error bars indicate the standard error of the means. For light from above and below, results show that increasing concentration decreases the initial wavelength of

261 the instability. In the absence of any other obvious trend, a linear regression analysis
262 is used to fit a straight line to the data (Table 2).
263

| **Experiment** | **Linear fit** | $R$ | $R^2$ | $p$ (constant) | $p$ (gradient) |
|---|---|---|---|---|---|
| CA | $0.316-1.48 \times 10^{-8} C$ | -0.849 | 0.721 | <0.0001 | <0.0001 |
| CB | $0.246-1.39 \times 10^{-8} C$ | -0.704 | 0.496 | <0.0001 | <0.0001 |

264 Table 2 Summary of linear regression statistics for concentration experiments. $R$ is the correlation
265 coefficient, $R^2$ is the coefficient of determination, $p$(constant) is the p-value associated with the constant
266 in the linear fit and $p$(gradient) is the p-value associated with the gradient coefficient in the linear fit
267 (calculated with ANOVA).
268
269 The correlation coefficients are both $R$<-0.7. The low p-values are highly significant
270 and indicate that it is very unlikely that there is not a correlation between the
271 concentration and initial wavelength. Using unpaired T-tests between consecutive
272 points for light from above gives $p$<0.05, highly significant. For light from below,
273 consecutive points give slightly insignificant p-values, but non-consecutive points
274 give highly significant values (for example, testing the first and the third points). Thus
275 together with the linear regression analysis, we conclude that there is negative
276 correlation between concentration and initial pattern wavelength.
277
278 **Does red light illumination affect the initial pattern wavelength?**
279 There is a considerably reduced response to light wavelengths greater than 550 nm in
280 the action spectra for the photo response of *Chlamydomonas* (Nultsch *et al*. 1971, for
281 *C. reinhardtii*); the photoresponse to red light is small. By illuminating a culture from
282 below using red light of wavelength 660 nm, we investigate whether initial pattern
283 wavelength varies with the light intensity. An example of the resulting patterns
284 formed with $I$=101 lux and a contour plot of the Fourier spectra with time are shown
285 in Fig. 3, and graphs of Fourier density are plotted in Fig. 5. In this particular
286 example, we note that the pattern does not appear everywhere in the dish at the same
287 time, possibly due to a remnant of mixing driven swirling. The dominant wavenumber
288 can still be extracted, and the double log fit is accurate.
289
290 In Fig. 6 there is no apparent trend in the wavelengths as the red light intensity is
291 varied. The correlation coefficient for linear regression, $R$=-0.0957 ($R^2$=0.009162), is

very small and implies that there is no significant correlation between the variables, and the corresponding p-values support this. In addition, no significance was found comparing the mean wavelength for different light intensities using sets of unpaired T-tests. This lack of response implies that illumination by red light is equivalent practically to no illumination, $I$=0 lux.

**White light illumination from below**

A significant phototactic response is elicited in *Chlamydomonas* for wavelengths between 370 and 550 nm (Nultsch et al. 1971), with a maximum at 503 nm and shoulder at 443 nm. Covering this range with the white LED array, results for the initial pattern wavelength as a function of illumination from below are shown for three independent experiments, with different cultures, in Fig. 7, with concentrations of $C$=5.35 x $10^6$ cells $cm^{-3}$, $C$=5.18 x $10^6$ cells $cm^{-3}$, and $C$=9.46 x $10^6$ cells $cm^{-3}$, and n=*6*, *n*=8, and n=8 in panels A, B and C, respectively. We denote these Experiment LB1, LB2 and LB3.

Results in Fig. 7 show the same trends: a decrease in initial wavelength as light intensity is increased to 2020 lux followed by an increase as intensity is increased to 2710 lux, and then what appears to be a stabilization of wavelengths as light is increased further, with wavelengths approximately constant beyond 2710 lux. If the data for red light for a similar concentration were included as $I$=0, it would also fit with the trend of decreasing wavelength as $I$ is increased to 2020 lux. As expected, there is some variability in the quantitative values of the mean wavelengths for different graphs, which may be due to the fact that slightly different concentrations are used, and cell behaviour may vary (i.e. variations in life or daily cycles). The trends found in these experiments are non-linear overall but appear to have quasi-linear regions. Thus we perform a linear regression separately on the first three points (for light intensities $I$=645, $I$=1330 and $I$=2020 lux) and then on the following four points ($I$=2710, $I$=3390, $I$=4080 and $I$=4770 lux), denoting the first three data points LB1a, LB2a and LB3a and the latter 4 points LB1b, LB2b and LB3b, for the three experiments, respectively. The linear fits and corresponding statistics are presented in Table 3.

| **Experiment** | **Linear fit** | $R$ | $R^2$ | $p$ (constant) | $p$ (gradient) |
|---|---|---|---|---|---|
| LB1a | $0.178-1.94 \times 10^{-5} I$ | -0.720 | 0.518 | <0.002 | <0.002 |
| LB2a | $0.208-2.68 \times 10^{-5} I$ | -0.650 | 0.422 | <0.002 | <0.002 |
| LB3a | $0.190-2.68 \times 10^{-5} I$ | -0.613 | 0.376 | <0.002 | <0.002 |
| LB1b | $0.164-9.62 \times 10^{-7} I$ | -0.066 | 0.0043 | <0.0001 | 0.760 |
| LB2b | $0.174-3.74 \times 10^{-6} I$ | -0.166 | 0.0274 | <0.0001 | 0.391 |
| LB3b | $0.157-2.87 \times 10^{-7} I$ | -0.015 | 0.0002 | <0.0001 | 0.934 |

Table 3 Summary of linear regression statistics for experiments with illumination from below. $R$ is the correlation coefficient, $R^2$ is the coefficient of determination, $p$(constant) is the p-value associated with the constant in the linear fit and $p$(gradient) is the p-value associated with the gradient coefficient in the linear fit (calculated with ANOVA).

For the first linear fit, Experiment LB1a shows the strongest negative correlation, while LB2a and LB3a show weaker correlations. The corresponding analysis of variance T-test gave a significance level of $p<0.002$ for the probability of being wrong in concluding that there is an association between light intensity and initial wavelength. Furthermore, unpaired T-tests on the first and the last data points in LB1a, LB2a and LB3a gave high significance levels, $p<0.05$, in every case. Thus we conclude that there is evidence of a significant linear negative correlation between light and wavelength for $I \leq 2020$.

For the second linear fit, the correlation coefficients are very low, especially for the more concentrated cells in LB3b and, hence, there is no evidence of a correlation between light intensity and wavelength for $I >2710$. In all cases the probability in being wrong in concluding that there is a relationship between the two variables is very high. Such statistics imply that these data sets are uncorrelated and that there is not sufficient evidence to conclude that light intensity, $I \geq 2710$ lux, and initial wavelength vary together in an associated way. Thus averaging all data points for $I \geq 2710$ in LB1b, LB2b and LB3b gives $\lambda_{WB1}=\lambda_{WB2}=0.1600$ (with s.d.=0.0115 and s.d.=0.0184, respectively) and $\lambda_{WB3}=0.1582$ (s.d.=0.0147).

The rise in $\lambda_0$ between $I$=2020 lux and $I$=2710 lux was examined using T-tests and found to be statistically significant in experiments LB1 and LB3, with $p<0.05$, but not significant in LB2. From this, together with the aforementioned statistical analysis, we

conclude that with increasing light intensity the initial wavelength decreases in a linear fashion, increases and stays at approximately the same level thereon in two cases and in the third case, decreases, stops decreasing and stays at approximately the same level. We shall interpret these results mechanistically in the discussion.

**White light illumination from above**

The initial pattern wavelength for cultures illuminated from above were explored in three experiments (using different cells), LA1, LA2 and LA3, with depth $H$=0.306 cm and concentrations $C$=5.05 x $10^6$ cells $cm^{-3}$, $C$=4.86 x $10^6$ cells $cm^{-3}$ and $C$=5.69 x $10^6$ cells $cm^{-3}$, respectively. Eight experimental runs were conducted for each light intensity, to establish the mean wavelength $\lambda_0$.

Results in Fig. 8, for initial wavelength versus light intensity, show the same trend: as light increases from 645 to 1330 lux the initial wavelength increases; beyond $I$=2020 lux, $\lambda_0$ decreases. If the data for illumination with red light for a similar concentration were included ($I$=0 lux, $\lambda_0$=0.19 cm), it would be consistent with the trend of increasing $\lambda_0$ for small $I$. As for illumination from below, the curves are qualitatively similar, but there are quantitative differences between the data sets due to the distinct cell populations.

Comparing the mean wavelengths for $I$=675 and $I$=1330 lux using an unpaired T-test it was found that the increase in wavelength was significant, with $p$<0.05, in every experimental case. Furthermore, a linear regression analysis was performed excluding the first data point, $I$=645 lux. The linear regression statistics are shown in Table 4. The negative correlation was strongest in LA1, and not as pronounced in LA2 and LA3. Using an unpaired T-test the difference in $\lambda_0$ for $I$=1330 and $I$=4770 lux was found to be significant in all three experiments, with 0.0001<$p$<0.0013. This, together with the small p-values found for all data sets (using ANOVA) for the probability of being wrong in concluding an association between the variables, indicates that the decrease in initial wavenumber as $I$ increases from 1330 lux to 4770 lux is a significant trend that is approximately linear.

| **Experiment** | **Linear fit** | *R* | $R^2$ | *p (*constant*)* | *p (*gradient*)* |
|---|---|---|---|---|---|
| LA1 | 0.285-2.78 x $10^{-5}$ *I* | -0.915 | 0.837 | <0.0001 | <0.0001 |
| LA2 | 0.272-1.59 x $10^{-5}$ *I* | -0.604 | 0.351 | <0.0001 | <0.0001 |
| LA3 | 0.299-1.97 x $10^{-5}$ *I* | -0.688 | 0.474 | <0.0001 | <0.0001 |

Table 4 Summary of linear regression statistics for illumination from above experiments. *R* is the correlation coefficient, $R^2$ is the coefficient of determination, *p(*constant*)* is the p-value associated with the constant in the linear fit and *p(*gradient*)* is the p-value associated with the gradient coefficient in the linear fit (calculated with ANOVA).

## Exploring the time to pattern formation

The time from mixing to pattern onset, $t_0$, as a function of light intensity was investigated. For red light, eight runs from Experiment RA, where *I*=325 lux, provided the mean $t_0$. For white light from above and below, two sample experiments, LA1 and LB1, were chosen and the mean $t_0$ calculated over eight runs for each light intensity, as plotted in

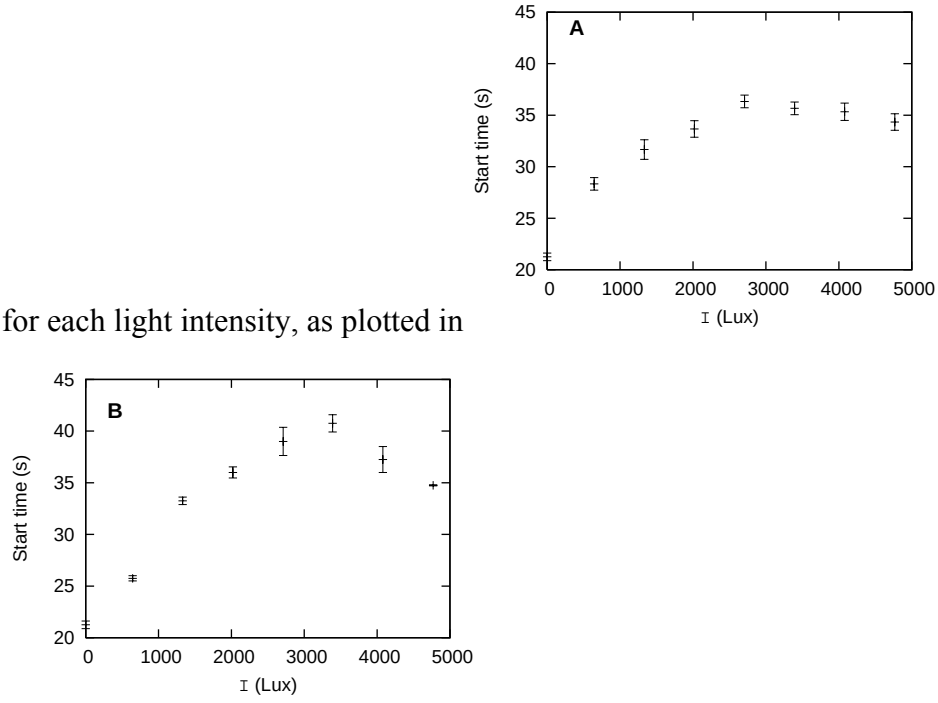


**Fig. 9**.

For Experiment LB1, the time to pattern formation increased from $t_0$=28 s at *I*=645 lux to a maximum of $t_0$=36 s at *I*=2710 lux. As *I* increase above 2710, the time to pattern formation then dipped a little to 34 s. For Experiment LA1, we see a similar pattern of behaviour except that the maximum occurs at 3390 lux with $t_0$=41 s. With red light, pattern formation occurred after 21 s, earlier than for any white light. If red

light is treated as $I$=0 then this datum point supports the above trends

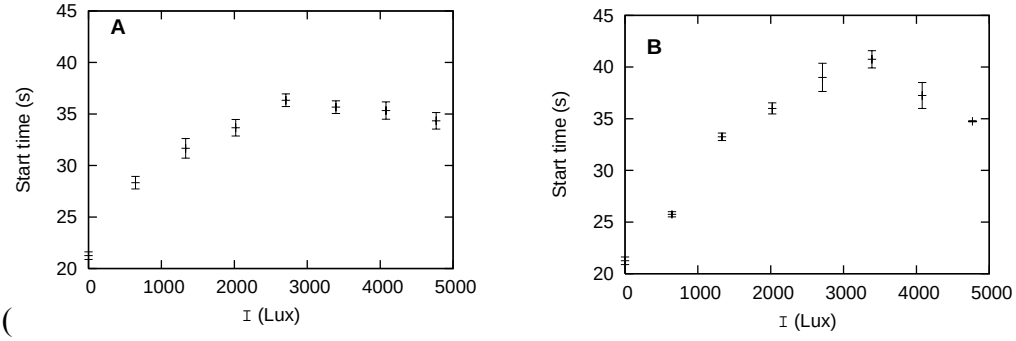


(**Fig. 9**).

## DISCUSSION

For a given light intensity, when the culture was illuminated from above or below, the initial wavelength of the most dominant mode, $\lambda_0$, decreased as concentration increased. This is consistent with the results of (Bees and Hill, 1997), with wavelengths of a similar order, supporting the hypothesis that increased gyrotaxis for higher cell concentrations encourages more focused and closely packed plumes.

The insensitivity of initial wavelengths to the red light illumination shows that, in terms of pattern formation at least, the cells do not exhibit a photo-response to light of wavelength 660 nm. This observation is consistent with data on individuals (Nultsch *et al*., 1971). Hence, red light is equivalent practically to no illumination. The average wavelength over all intensities for red light is $\lambda_0$=0.19 cm, which is of the same magnitude as similar experiments (Bees and Hill, 1997), although a little smaller (57.4% of the reported value for concentration $C$=3.6 x $10^6$ cells/cm$^{-3}$ and depth $H$=0.324 cm in Bees and Hill, 1997).

We have reported the first statistically significant trends for initial pattern wavelength as a function of white light intensity for cultures illuminated either from above or below. The results for both light orientations were found to be repeatable. Distinct transitions were observed as the light intensity was increased. To explain these results, we recall that there is a competition between bottom-heavy induced upswimming (gravitaxis), gyrotaxis due to viscous and gravitational torques, and phototaxis towards/away from weak/bright light, distinguished by the critical light intensity, $I_c$.

For the case of illumination from below (Fig. 7), the initial wavelength decreased linearly as light intensity was increased from $I$=645 to 2020, then increased as intensity increased from 2020 to 2710, and remained constant for $I \geq 2710$ lux. From these results, it would appear that $2020 \leq I_c \leq 2710$ lux. For very weak illumination, cells generally swim upwards, but the probability density function (pdf) for the orientation of cells will be less biased upwards as $I$ increases, and cells will be more responsive to viscous torques, leading to stronger gyrotaxis (swimming towards regions of downwelling fluid), more focussed plumes and thus smaller wavelength instabilities. (Note that gyrotaxis can induce linear instabilities of small wavelength even in suspensions of uniform concentration.) With illumination from below for $I<I_c$, shading does not permit a steady state with a maximum within the suspension. For $I$ just below $I_c$, photo-gyrotaxis plays a critical role as short wavelength instabilities develop before gravitationally stable steady states are attained (cells concentrated at the bottom). For $I>I_c$, cells typically swim upwards, leading to accumulations at the upper surface and overturning instabilities with circulation associated with the whole fluid layer ($\lambda_0$ does not change significantly with $I$). It is the switch from a photo-gyrotactic instability from an evolving basic state to an overturning instability from photo-gravitaxis that provides the rapid change in wavelengths in Fig. 7.

With light from above (Fig. 8), the initial wavelength increased a little with light intensity between 645 and 1330 lux, and decreased between 1330 and 4700 lux. To explain the former, for weak illumination the cells swim towards the light on average and, hence, gravitaxis is supported by phototaxis. Greater illumination, shaded by cells from above, leads to a broader less concentrated accumulation of cells at the upper surface away from the constraining upper boundary, which can induce instability with a greater wavelength. When $I$ is increased above $I_c$, negative phototaxis is sufficient to overcome negative gravitaxis (Häder, 1987), and the cells near the top of a uniform suspension swim downwards, whilst those lower down swim upwards due to shading, in theory creating a concentrated sublayer somewhere within the full layer. Since the sublayer is denser than the suspension below, a stable region overlies an unstable region. We propose a dual explanation for the decrease in pattern

464 wavelength as white light intensity increases further. Firstly, the disposition of cells
465 near the light source to swim downwards as the intensity increases broadens the
466 orientation pdf thus increasing gyrotactic focussing, which decreases $\lambda_0$. Secondly, as
467 light intensity increases, the unstable region below the sublayer decreases in size,
468 stabilizing large wavelength instabilities more than small. To determine the critical
469 light intensity $I_c$ from above, note that zero phototaxis typically occurs at two points:
470 $I$=0, $I_c$. Therefore, one might expect $\lambda_0$ to be the same at both. Of course, self-
471 shading within the suspension, particularly at the top, complicates the argument and
472 limits the accuracy of this prediction, although the results are consistent with
473 illumination from below, with Fig. 8 yielding a value of $I_c$≈3000.
474
475 The start time of pattern formation, $t_0$, was computed as a function of illumination
476 from above or below. For red light, instabilities typically are seeded by unstable cell
477 concentration profiles and gyrotaxis supports the process. For low light intensities
478 with light from below, cells swim downwards as light intensity increases, delaying the
479 time to form an unstable density gradient and thus initiate instability, despite the
480 amplified gyrotaxis. For $I$ >2710 lux, overturning instabilities near the upper
481 boundary are the dominant mechanisms, taking a while to form as they will not be
482 supported by gyrotaxis. Similarly, illumination from above presents an analogous
483 competition of taxes.
484
485 **Comparison with theoretical predictions of photo-gyrotactic bioconvection**
486 An aim of this study is to present results that can be compared with current and future
487 theoretical predictions. In theory, initial wavelength predictions can be compared.
488 However, such a comparison is rarely straightforward (see later) and there are some
489 key issues that need to be addressed: have the effects of mixing sufficiently
490 diminished before pattern formation begins, and has the cell distribution approached
491 the theoretical steady state before pattern onset? To answer the first question, we
492 assume that the Petri dish is in solid body rotation with angular velocity $|\boldsymbol{\Omega}|$ until the
493 mixing stops and the container instantaneously comes to rest (Hill *et al*., 1989; Bees
494 and Hill, 1997). The time for spin down and decay of fluid motion is $O(E^{-1/2}\ |\boldsymbol{\Omega}|^{-1})$,
495 where $E=\nu(|\boldsymbol{\Omega}|\ H^2)^{-1}$ is the Ekman number, $\nu$ is the viscosity and $H$ is the layerdepth
496 (REF--------). In our case, $|\boldsymbol{\Omega}|$= 21 $s^{-1}$ (using the speed of the vortex mixer), and we

497 calculate $E$=5.3x10$^{-3}$, thus $O(E^{-1/2}\ |\mathbf{\Omega}|^{-1})$=0.65 s. Since pattern formation starts after
498 tens of seconds, we conclude that the flow is likely to have diminished sufficiently.
499 For a mean cell swimming speed of 63 μm s$^{-1}$ (Hill and Häder, 1997), with an upward
500 bias of 56% (Bees *et al.*, 1998), then if the layer is 0.3 cm deep a cell takes 43 s to
501 swim half the depth. This implies that not all the cells will have had sufficient time to
502 form the steady states used in the models. However, some qualitative comparisons can
503 still be drawn.
504
505 Recent theory employs linear stability analyses to assess the initial pattern
506 wavelengths of instabilities in both gyrotactic-only (Pedley and Kessler, 1990; Bees
507 and Hill, 1998) or phototactic-only cells (Vincent and Hill, 1996). Results for red
508 light can be compared with gyrotaxis only models, and trends for the effects of white
509 light on initial bioconvection wavelengths can be compared with predictions from
510 photo-gyrotactic models (Williams and Bees, 2010). Three models for photo-
511 gyrotaxis have recently been presented and explored in detail (*idem*). For simplicity
512 near criticality and in the absence of definitive information to the contrary, in Model
513 A, mean cell swimming speed decreases linearly with $I$, with zero mean swimming at
514 the critical light intensity, $I_c$. The mean cell swimming direction is determined
515 separately by balancing gravitational and viscous torques in a stochastic formulation.
516 In Model B, each cell's deterministic-stochastic ratio varies linearly with $I$, effectively
517 via its centre-of-mass offset: at $I$=$I_c$, the gravitational torque is zero and in the absence
518 of viscous torques the cell is equally likely to swim in all directions; for $I$<$I_c$, the cell
519 swims upwards on average, obtaining the measured value for $I$=0. In Model C, an
520 effective phototactic torque (e.g. due to an active asymmetric adjustment of the
521 flagellar beat) complements the existing gravitational and viscous torques; the model
522 displays evidence of novel non-hydrodynamic modes. Since fluid flow was integral
523 to the results obtained experimentally, only comparisons with Models A and B are
524 made here: a layer of finite depth illuminated from above is studied, where key
525 parameters are the scaled layerdepth, $d$, the ratio of the light intensity at the source, $I_s$,
526 to the critical light intensity, $\chi$=$I_s$/$I_c$, and the Rayleigh number, $R$=v$g\Delta\rho H^3 dN/(v\rho V_n^2\tau)$,
527 which is a ratio of the destabilising to stabilising forces (see Bees and Hill, 1998).
528 Here, v, $\rho$, $V_n$ and $\tau$ are cell volume, density, mean swimming speed and direction
529 correlation time, respectively, $\Delta\rho$ is the difference between cell and fluid density, $g$ is

530 the gravitational acceleration and $N$ is the scaled mean cell concentration (Williams
531 and Bees, 2010). The case $\chi$=0 is for zero or red light; a gyrotaxis-only model (Bees
532 and Hill, 1998). Increasing $\chi$ is equivalent to increasing light intensity, however $I_c$ is
533 not known, so quantitative conversion between the two is not possible. The linear
534 stability analysis provides an estimate for the critical Rayleigh number, $R_c$, and
535 corresponding critical wavenumber $k_c$; for $R<R_c$ small perturbations decay; for $R$ just
536 greater than $R_c$, instabilites develop with a wavenumber of $k_c$. (Note: the critical
537 dimensional wavelength, $\lambda_c$, is given by $2\pi H/k_c$.) Experiments provide an estimate of
538 the dominant initial wavelength, $\lambda_0$, which has a non-zero growth rate and occurs for
539 some $R>R_c$. We may compare the predicted critical wavelength $\lambda_c$ at $R=R_c$ with the
540 fastest growing wavenumber, $\lambda_0$, as experimental $I$ or theoretical $\chi$ are varied, as long
541 as $R$ is not too much greater than $R_c$.
542

| **Experiment** | $H$ (cm) | $I$ (lux) | $\lambda_0$ (cm) | $R$ x$10^6$ |
|---|---|---|---|---|
| RA | 0.306 | Any/0 | 0.190 | 2.18 |
| LA1 | 0.306 | 645 | 0.235 | 2.18 |
| LA1 | 0.306 | 1330 | 0.256 | 2.18 |
| LA1 | 0.306 | 2020 | 0.228 | 2.18 |
| LA1 | 0.306 | 2710 | 0.201 | 2.18 |
| LA1 | 0.306 | 3390 | 0.188 | 2.18 |
| LA1 | 0.306 | 4080 | 0.170 | 2.18 |
| LA1 | 0.306 | 4780 | 0.159 | 2.18 |
| **Theory:** | | $\chi$ | $\lambda_c$ (cm) | $R_c$ x$10^6$ |
| No light | 0.306 | 0 | 0.042 | 2.77 |
| Model A/B | 0.306 | 0.6 | 0.154/0.381 | 1.32/0.717 |
| Model A/B | 0.306 | 1.0 | 0.345/0.432 | 0.402/0.317 |
| Model A/B | 0.306 | 1.2 | 0.345/0.457 | 0.271/0.236 |
| Model A/B | 0.306 | 1.4 | 0.106/0.136 | 10.9/11.6 |
| Model A/B | 0.306 | 1.45 | 0.051/0.062 | 36.3/39.5 |
| Model A/B | 0.306 | 1.5 | 0.031/0.037 | 91.6/101.0 |

543 Table 5 Summary of experimental results and theoretical predications, with light from above.
544

For the comparison we fix $H$=0.306 cm and the direction correlation time $\tau$=5 s (Bees and Hill, 1997); the gyrotactic reorientation timescale $B$=6.3 s (Jones *et al*., 1994); and the dimensional measure of absorbance $\alpha$=3.67 x $10^7$ $cm^2$ (*C. augustae*: colorimeter measurement). Using these parameters, the theoretical predictions provide $\lambda_c$ and $R_c$, which are shown along with the experimental data in Table 5.

We find promising consistency between theoretically predicted critical wavelengths and experimentally observed dominant initial wavelengths. The critical wavelength in the dark is $\lambda_c$=0.042 ($R_c$=2.77 x $10^6$), which is around a factor of 4 lower than the measured wavelength $\lambda_0$=0.190 for red light data (at a fixed $R$=2.18 x $10^6$). Models A and B predict an increase in $\lambda_c$ initially with increasing $\chi$ followed by a decrease for some value of $\chi$>1, a trend also seen in the experimental data for $\lambda_0$ as $I$ increases (compare Fig. 8 and Fig. 10). The critical wavelength does not vary much once the maximum value of $\lambda_c$ is reached, until $\chi$>1.25. The maximum critical wavelength and critical Rayleigh number are $\lambda_c$ =0.345 cm and $R_c$ =1.49 x $10^5$ in Model A, and $\lambda_c$ =0.457 cm and $R_c$ =2.20 x $10^5$ in Model B. In the experimental data the maximum $\lambda_0$ ranged from 0.244-0.262 cm for $I$=1330 lux over the three experiments. In Models A and B the critical wavelength decreases rapidly and nonlinearly as $\chi$>1.25 increases. The analogous decrease in $\lambda_0$ is linear in the experiments. This may be due to the models having the same critical light intensity, $I_c$, for all cells, whereas a natural distribution of $I_c$ in experiments would act to smooth the transition. We see a larger range for $\lambda_c$ than was found experimentally for $\lambda_0$, which may in part be due to the fact that the critical wavelength is not necessarily representative of the fastest growing mode, especially true for large critical wavelengths (small wavenumbers).

To conclude, comparisons between theoretical and experiment results are difficult and there are many limitations. Experimentally identifying the very first dominant wavelength can be difficult, and there will always be remnants of the mixing. Theoretically, the prediction of $\lambda_c$ comes from finding a steady distribution and perturbing, but there may not be sufficient time for the formation of this state. The aim of the work was to explore mechanisms rather than using parameter fitting methods. We have observed qualitative agreement between experiments and theory, and anticipate quantitative alignment once better parameter measurements are obtained and the theoretical analyses refined.

## Conclusions

In this paper, we have developed and employed techniques to quantify the initial pattern wavelength of bioconvection as a function of concentration and light intensity in a repeatable fashion. A novel mixing methodology was developed to create a consistently uniform distribution before the onset of pattern formation. In practise, this is a difficult task and the distribution is never uniform: the mixing can never be perfect and the swimming behaviour of the cells relative to the fluid flow induces memory. However, the employed on-off series of rotations were vigorous, inducing large amplitude flows that decayed rapidly and mixing the cells well and quickly. In all but a few cases where pattern formation was rapid (very high concentrations), the patterns did not display any structure associated with remnants of the mixing protocol, and developed from a steady and uniform suspension. Furthermore, the mixing regime ensures that the initial conditions are at least consistent between runs, allowing changes in the wavelength to be attributed to culture parameters. Future work could attempt to quantify the mixing (but note that it does not follow that the mixing of tracer particles is equivalent to the mixing of gyrotactic swimming cells).

Images were captured and the dominant initial pattern wavelength was extracted using Fourier analysis. The trend in initial wavelength as a function of concentration was similar to that found previously (Bees and Hill 1997). Red light illumination at 660 nm was found to have no effect on initial pattern wavelength. However, significant trends for initial wavelength as a function of white light illumination from either above or below were discovered, analysed and interpreted. In particular, the competition between gravitaxis, gyrotaxis and phototaxis proved to be fundamental to the pattern forming process. Comparisons between a new photo-gyrotactic theory (Williams and Bees, 2010; incorporating the Lambert-Beer law for light absorption) and these experimental results were made, indicating some good agreement. To extend the comparison to long-term pattern wavelengths for the photo-gyrotactic system, it will be necessary to take into account the likely nonlinear scattering that will occur locally within down welling plumes with significantly higher cell concentration than the mean. Refinement of the trends around what appear to be the critical values of $I$ should also be explored to try and provide an accurate estimate of $I_c$. Techniques should be developed to analyse geometrical aspects of the patterns

under different illumination conditions, and so elucidate the mechanisms at play during photo-gyrotactic bioconvection.

## LIST OF SYMBOLS AND ABBREVIATIONS

| | |
|---|---|
| ANOVA | Analysis of variance |
| BBM | Bold's basal medium |
| FFT | Fast Fourier transform |
| $k_0 / k_c / k_d$ | Initial / critical / dominant wavenumber |
| $\lambda_0$ | Initial wavelength |
| $t_0$ | Time from mixing to pattern formation |
| $C$ | Concentration |
| $D$ | Scaled layerdepth |
| $E$ | Ekman number |
| $H$ | Depth of layer |
| $I$ ( $I_c$) | (Critical) light intensity |
| $R$ ( $R_c$) | (Critical) Rayleigh number |
| $W_I$ | Image width |
| $\tau$ | Direction correlation time |
| $\alpha, \beta, c$ | Fitting parameters in the double logarithmic function |
| $\lvert\boldsymbol{\Omega}\rvert$ | Vortex mixer speed |
| $\chi$ | Dimensionless ratio of critical to source intensity |

## ACKNOWLEDGEMENTS

The authors gratefully acknowledge support from the EPSRC (EP/D073398/1).

## REFERENCES

**Bees, M. A.** (1996)**.** Non-linear pattern generation in suspensions of swimming micro-organisms. PhD thesis, University of Leeds.

**Bees, M. A. and Hill, N. A.** (1997). Wavelengths of bioconvection patterns. *J. Exp. Biol.* **200**, 1515-1526.

**Bees, M. A. and Hill, N. A.** (1998). Linear bioconvection in a suspension of randomly swimming, gyrotactic micro-organisms. *Phys. Fluids* **10**, 1864-1881.

627 **Bees, M. A., Hill, N. A., and Pedley, T. J.** (1998). Analytical approximations for the
628 orientation distribution of small dipolar particles in steady shear flows. *J. Math. Biol.*
629 **36**, 269-298.

630 **Childress, S., Levandowsky, M., and Spiegel, E. A.** (1975). Pattern formation in a
631 suspension of swimming microorganisms: equations and stability theory. *J. Fluid*
632 *Mech*. **69**, 591-613.

633 **Czirók, A., Janosi, I. M., and Kessler, J. O.** (2000). Bioconvective dynamics:
634 dependence on organism behaviour. *J. Exp. Biol.* **203**, 3345-3354.

635 **Ghorai, S. and Hill, N. A.** (2005). Penetrative phototactic bioconvection. *Phys.*
636 *Fluids* **19**, 74-101.

637 **Häder, D. P.** (1987). Polarotaxis, gravitaxis and vertical phototaxis in the green
638 flagellate, *Euglena gracilis. Arch. Microbiol.* **147**, 179-183.

639 **Hill, N. A. and Häder, D. P.** (1997). A biased random walk model for the trajectories
640 of swimming micro-organisms. *J. Theor. Biol.* **186**, 503-526.

641 **Hill, N. A., Pedley, T. J., and Kessler, J. O.** (1989). Growth of bioconvection
642 patterns in a suspension of gyrotactic micro-organisms in a layer of finite depth. *J.*
643 *Fluid Mech*. **208**, 509-543.

644 **Jones, M. S., le Baron, L. and Pedley, T. J.** (1994). Biflagellate gyrotaxis in a shear
645 flow. *J. Fluid Mech.* **281**, 137-158.
646
647 **Kessler, J. O.** (1984). Gyrotactic buoyant convection and spontaneous pattern
648 formation in algal culture. In: *Non-equilibrium cooperative phenomena in physics and*
649 *related fields* (ed. Verlarde, M. G.), pp. 241-248. New York, Plennum.

650 **Kessler, J. O.** (1985a). Co-operative and concentrative phenomena of swimming
651 micro-organisms. *Contemp. Phys.* **26**, 147-166.

652 **Kessler, J. O.** (1985b). Hydrodynamic focusing of motile algal cells. *Nature* **313**,
653 218-220.

654 **Kessler, J. O.** (1986). The external dynamics of swimming micro-organisms. *Prog*.
655 P*hycol. Res.* **4**, 258-305.

656 **Kessler, J. O., Hill, N. A. and Häder, D. P.** (1992). Orientation of swimming
657 flagellates by simultaneously acting external factors. *J. Phycol.* **28**, 816-822.
658
659 **Nultsch, W., Throm, G., and von Rimscha, I.** (1971). Phototaktische
660 untersuchungen an *Chlamydomonas reinhardii* dangeard in homokontinuierlicher
661 kultur. *Arch. Mikrobiologie* **80**, 351-369.

662 **Pedley, T. J. and Kessler, J. O.** (1990). A new continuum model for suspensions of
663 gyrotactic micro-organisms. *J. Fluid Mech*. **212**, 155-182.

664 **Platt, J. R.** (1961). "Bioconvection Patterns" in Cultures of Free-Swimming
665 Organisms. *Science* **133**, 1766-1767.

666 **Veronis, G.** (1963). Penetrative convection. *J. Astrophys.* **137**, 641-663.

667 **Vincent, R. V. and Hill, N. A.** (1996). Bioconvection in a suspension of phototactic
668 algae. *J. Fluid Mech.* **327**, 343-371.

669 **Wager, H.** (1911). On the effect of gravity upon the movements and aggregation of
670 *Euglena viridis*, Ehrb. and other micro-organisms. *Phil. Trans. R. Soc. Lond. B* **203**,
671 333-390.

672 **Williams, C. R.** (2009). Pattern formation and hydrogen production in suspensions of
673 swimming green algae. PhD thesis, University of Glasgow.
674
675 **Williams, C. R. and Bees, M. A.** (2010). Photo-gyrotactic bioconvection. *J. Fluid*
676 *Mech.* (submitted).
677
678

## FIGURES AND FIGURE LEGENDS

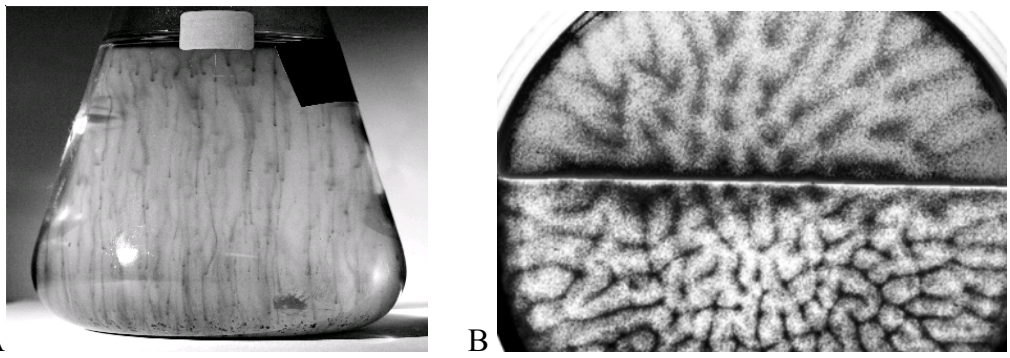


Fig. 1 A) Gyrotactic plumes in a culture flask. B) Bioconvection patterns in a Petri dish (depth 0.4 cm; width 5 cm; $10^6$ cells $cm^{-3}$): the illumination is white from below; the lower half is covered with a red filter (660 nm; contrast enhanced). The two regions display different bioconvection patterns: in the top half, white illumination leads cells to swim upwards, with phototaxis supporting gravitaxis and suppressing gyrotaxis, initiating an overturning instability with broad downwelling structures; in the bottom half, cells do not respond to the red illumination and form finely focused gyrotactic plumes.

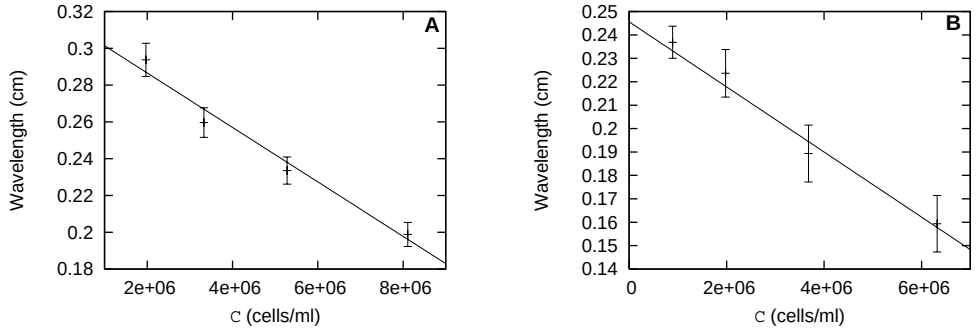


Fig. 2 The effects of concentration on dominant initial pattern wavelength. A) Experiment CA, culture illuminated from above with a white light: $I$=645 lux; $H$=0.306 cm. B) Experiment CB, culture illuminated from below with a white light: $I$=645 lux; $H$=0.345 cm.

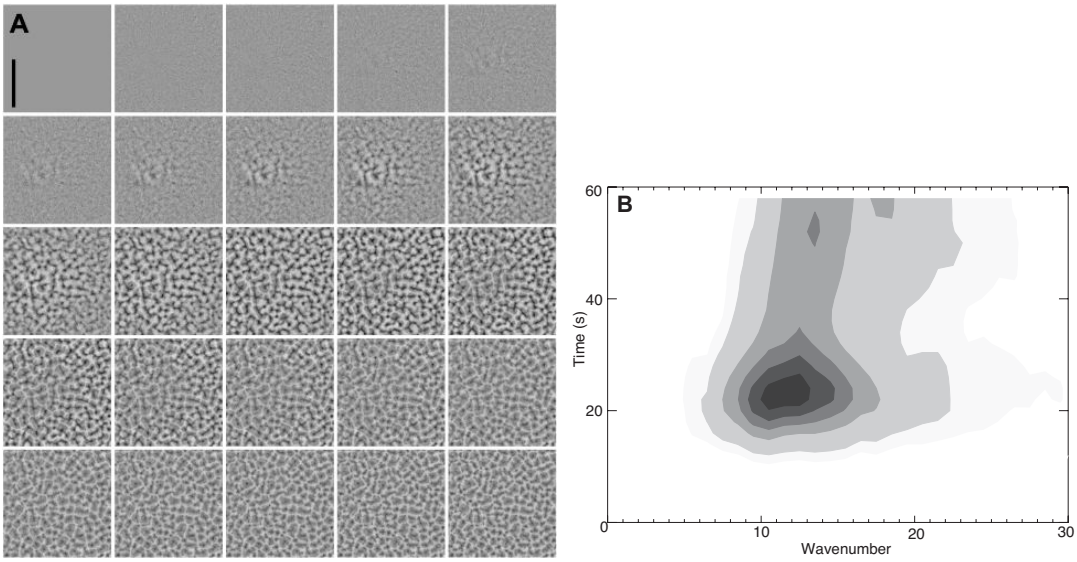


Fig. 3 Sample results from Experiment RA, with red light illumination from above: $I$=101 lux; $C$=5.05 x $10^6$ cells $cm^{-3}$; $H$=0.306 cm; $W_I$=2.33 cm. A) Images every 2 s, starting 10 s after mixing. B) Contour plot of the Fourier spectrum, where time is measured from the start of image recording (not the time since mixing). Scale bar: 1cm.

698

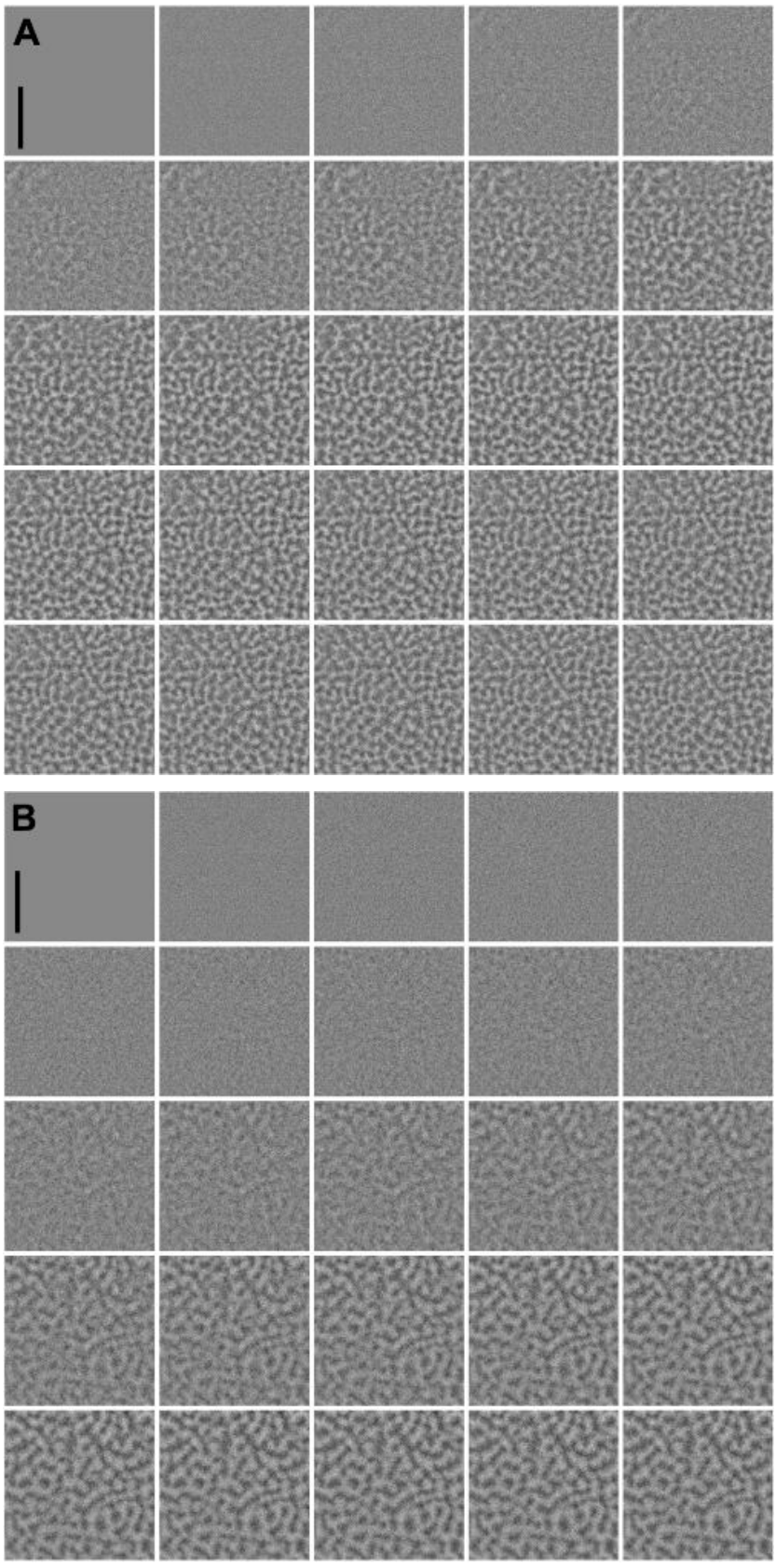


699

700

701 Fig. 4 Sample images from Experiment CA: white light illumination from above, I=645 lux; H=0.306
702 cm; $W_I$=2.47 cm. A) C=8.11 x $10^6$ cells $cm^{-3}$ and B) C=3.33 x $10^6$ cells $cm^{-3}$. Images were captured
703 every 2 s, starting 10 s after mixing. Scale bar: 1cm.

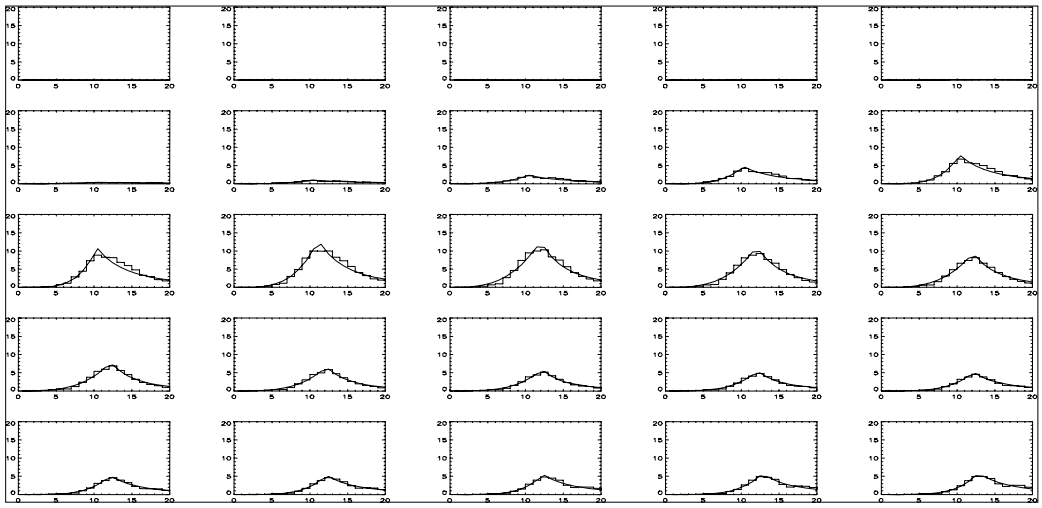

Fig. 5 Fourier spectra from Experiment RA, with red light illumination from above: $I$=101 lux; $C$=5.05 x $10^6$ cells $cm^{-3}$; $H$=0.306 cm. Spectra every 2 s, starting 10 s after mixing ended. The horizontal axis is wavenumber and the vertical axis is Fourier density. Histograms represent binned data of the FFT spectrum of each processed pattern image, whereas the curves are produced from fitting Eqn. 1.

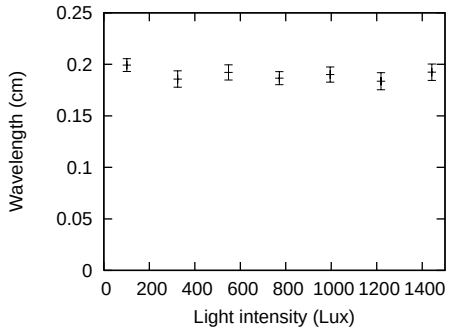


Fig. 6 The effect of red light from above on dominant initial pattern wavelength: H=0.306 cm; C=5.05 x $10^6$ cells $cm^{-3}$. Each point represents the mean of eight runs of Experiment RA; error bars are the standard error of the mean.

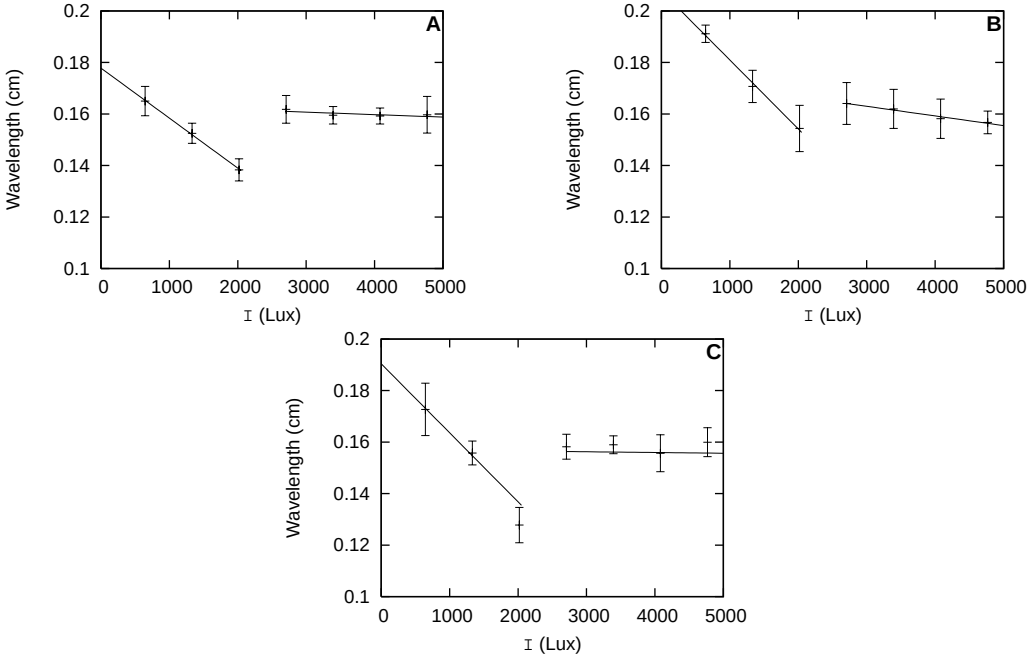


Fig. 7 The effect of white light illumination from below on dominant initial pattern wavelength: $H$=0.306 cm. A) $C$=5.35 x $10^6$ cells $cm^{-3}$; B) $C$=5.18 x $10^6$ cells $cm^{-3}$; C) $C$=9.46 x $10^6$ cells $cm^{-3}$. Each

point represents the mean of 6 runs of Experiment LB1 and 8 runs of LB2 and LB3; the error bars are the standard error of the mean. Linear regression fits have been plotted for all experiments, separately for the first three or last four points in each data set.

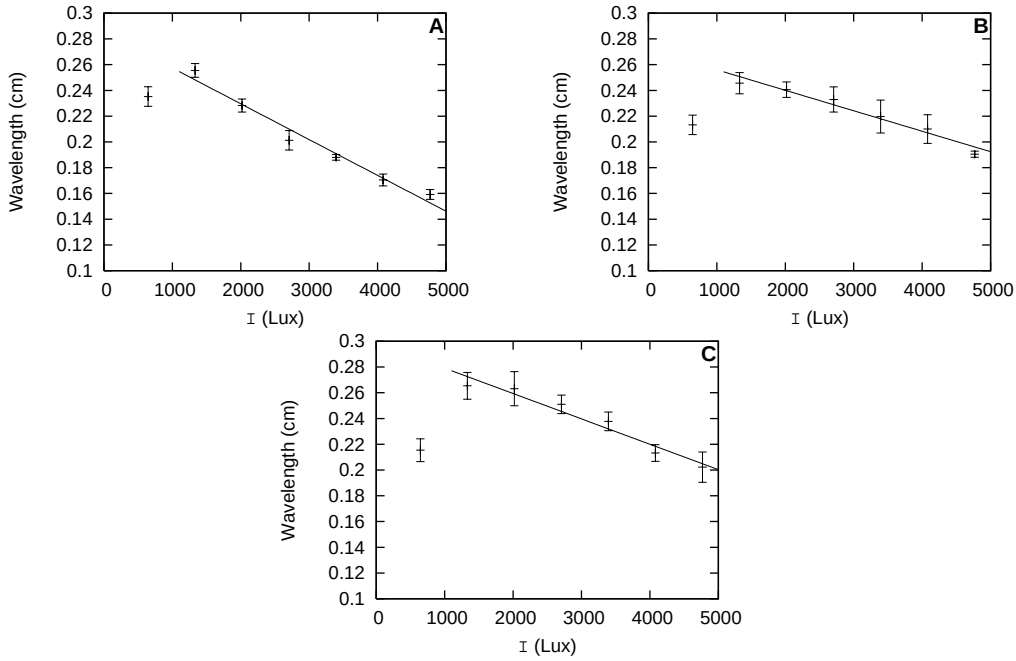


Fig. 8 The effect of white light illumination from above on dominant initial pattern wavelength: $H$=0.306 cm. A) $C$=5.05 x $10^6$ cells $cm^{-3}$; B) $C$=4.86 x $10^6$ cells $cm^{-3}$; C) $C$=5.69 x $10^6$ cells $cm^{-3}$. Each point represents the mean of 8 runs of Experiments LA; the error bars are the standard error of the mean. Linear regression fits have been plotted for all experiments (excluding the first datum point at $I$=645 lux in each).

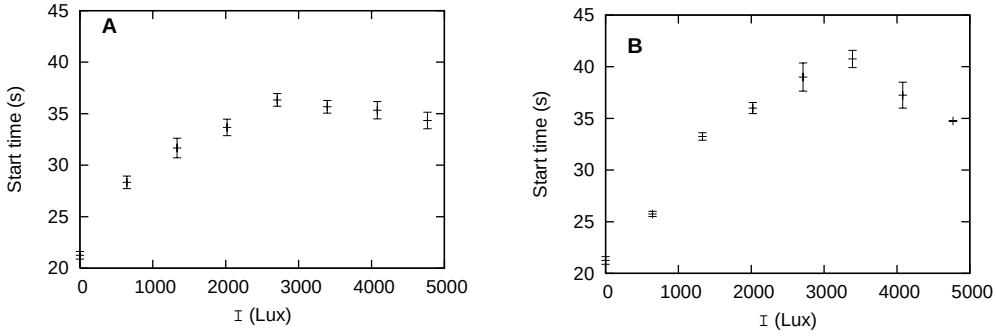


Fig. 9 Plots of mean initial start time, $t_0$, with light intensity, for A) Experiment LB1 and B) Experiment LA1. The mean start time for $I$=325 lux for the red light Experiment RA is included as $I$=0 lux: red light has negligible effect on photo-motility. $H$=0.306 cm; images were captured every 2 s, starting 12 s after mixing.

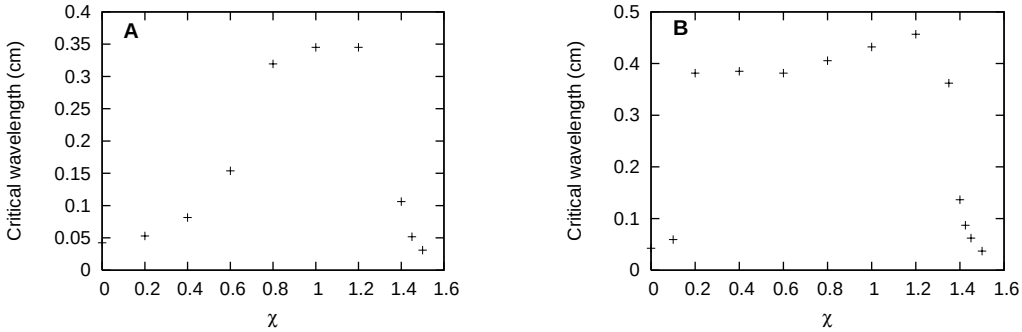


Fig. 10 Critical wavelength, $\lambda_c$, plotted against $\chi$. A) Model A; B) Model B. $H$=0.306; $\alpha$=3.67 x $10^7$ $cm^2$.